PCCP

Accepted Manuscript

ROYAL SOCIETY OF CHEMISTRY

www.rsc.org/pccp

Physical Chemistry Chemical Physics
CREATED USING THE RSC LaTeX PCCP ARTICLE TEMPLATE – SEE www.rsc.org/electronicfiles FOR DETAILS
ARTICLE TYPE www. rsc.org/xxxxxx | XXXXXXXX

Surface site coordination dependent responses resolved in free clusters: Applications for neutral sub-nanometer cluster studies

Lauri Hautala,*[a]‡ Kari Jänkälä,[a] Mikko-Heikki Mikkelä,[b] Maxim Tchaplyguine[b] and Marko Huttula[a]

Received Xth XXXXXXXXXX 20XX, Accepted Xth XXXXXXXXXX 20XX
First published on the web Xth XXXXXXXXXX 20XX
DOI: 10.1039/b000000x

In this paper we demonstrate how surface site specific experimental information can be obtained from free low nanometer scale clusters using photoelectron spectroscopy utilising synchrotron radiation. In addition, we show how it can be used to gain insight into the geometry and surface structure of the clusters. The present experiments were conducted on alkali metal halides RbCl and CsCl which were chosen as advantageous test cases due to their simple electronic and geometric structure. These heavy alkali metal salts provide additional clarity since the surface and bulk responses can be separated which is not the case for clusters of lighter alkali metal salts. Computational chemical shift calculations and simple alkali halide cluster size modelling were used to interpret the experimental results.

1 Introduction

Nanometer sized aggregates of matter - clusters have become compelling subjects to study in different areas of science such as physics [1], chemistry [2,3], medicine [4], and materials science [5]. Clusters are vitally important for processes occurring in atmosphere [6] and even in space [7]. When produced in laboratories, clusters with various novel properties provide building blocks for nanomaterials where, for example, catalytic properties can be tuned at sub-nano scale [8,9].

One of the most curious features of clusters is their ability to change physical and chemical properties as a function of size and geometry [2–5,8]. This capability can, to a significant extent be assigned to the changing relative abundances of dissimilarly coordinated atoms. The most obvious division can be made between atoms located at the surface and in the bulk of the clusters. In addition, atoms in the surface layer can have different coordination depending on their position. For a given cluster size and geometry it is possible to calculate the number of atoms at each coordination site. As the cluster size changes, the relative abundance of atoms in different sites varies.

Core-level photoelectron spectroscopy using synchrotron radiation is a powerful experimental technique which allows to gain site specific information about the structure of nanoscale clusters [10,11]. Core-level electrons are affected by the presence of site-specific chemical environment, which causes so-called chemical shifts to the electron binding energies [12]. By determining the chemical shifts using photoelectron spectroscopy one can probe the local electronic structure of the object in question.

In certain cases the responses from atoms located at the cluster surface and in the bulk can be separated in photoelectron spectra [13,14]. Moreover, theoretical calculations on clusters [15,16] have predicted that surface atoms at the sites with different coordination should also exhibit noticeably dissimilar binding energies. Resolving these site specific responses experimentally would provide valuable information about the cluster properties important, for example, in the studies of photochemical activity and catalysis. As the site abundances relate directly to the arrangement of atoms in clusters, this could also be used as a probe to the cluster geometry [15]. There have been attempts to assign the core-level photoelectron spectra of Kr and Xe clusters using multipeak fitting in order to extract site specific information with some success [10,17]. In these studies, the cluster surface response has been seen to consist of several responses originating from different surface sites but in most other cases, the surface site resolution has remained modest.

In the present article we report an experimental study where *surface site* resolved core-level photoelectron spectra from free neutral RbCl and CsCl clusters in the sub- and low-nanometer size range were recorded using synchrotron radiation. Intensity of the site specific responses are seen to evolve as a function of the cluster size. The changes in the spectra are interpreted as reflecting the geometry of the clusters in question. The validity of our assignments has been also compared to results obtained by using chemical shift calculations and simple alkali halide cluster size estimation procedure. A dis-

[a] *Department of Physics, University of Oulu, P.O. Box 3000, 90014 University of Oulu, Finland.*
[b] *MAX IV Laboratory, Lund University, Box 118, 22100 Lund, Sweden.*
‡ *E-mail: lauri.hautala@oulu.fi*

cussion concerning the general findings of site resolved photoelectron spectroscopic studies of clusters based on the experimental and computational results is presented.

2 Experiments

2.1 Description of the experiments

The alkali halide clusters were produced using the so-called Exchange Metal Cluster (EXMEC) source. Its operation is based on a pick-up principle where a primary beam of inert-gas clusters created by an adiabatic expansion source acts as a growth platform for dopant atoms or molecules. A detailed description of the source has been presented earlier (see Ref. [18]) and only the main operation parameters are given here. In addition to metal clusters, EXMEC has been used to produce small neutral clusters of several different elements and compounds [16,19,20].

In the cluster source, argon gas of controlled stagnation pressure was expanded into vacuum through a liquid nitrogen cooled nozzle with a throat diameter of 150 μm and half-opening angle of 10°. The cluster beam travelled a distance of about 12 mm from the nozzle to a conical copper skimmer with an orifice diameter of 300 μm. After the skimmer, the Ar clusters entered a 10 mm long pick-up oven leading to pick-up events between the vaporised alkali halide monomers and Ar clusters. RbCl and CsCl powders (Sigma Aldrich, 99.95 % purity) were evaporated using inductively and resistively heated ovens, respectively. Agglomeration of alkali halide monomers occurs while the Ar cluster acts as a thermal bath dissipating the heat released by the monomer-cluster collisions and alkali halide cluster formation.

After the pick-up oven, the cluster beam crosses ionising x-ray radiation and electrons emitted from the clusters as a result of a photoionisation process are detected. Measurements were performed at the synchrotron radiation facility MAX-lab (MAX IV Laboratory) in Lund, Sweden. The experiments were carried out at the undulator beamline I411 of the 1.5 GeV MAX II storage ring [21,22]. The emitted photoelectrons were detected by a Scienta R4000 hemispherical analyser attached to the end-station at the "magic-angle" of 54.7° with respect to the horizontally polarised synchrotron radiation and perpendicular to the cluster and photon beam.

During the experiments, the argon cluster size was kept constant by fixing the operation parameters (stagnation pressure and nozzle temperature) of the adiabatic-expansion source while the oven temperature was varied between 570 °C and 620 °C for RbCl and between 430 °C and 580 °C for CsCl. The Ar stagnation pressures and nozzle temperatures are tabulated in Table 1. With the given parameters, one can estimate the mean argon cluster size using the Hagena scaling parameter formalism [23,24]. These values are found in the upper half of Table 1. The variation of the predicted mean Ar cluster size was calculated based on the given error limits for the stagnation pressure and nozzle temperature. Note that the given error limits do not indicate the width of the Ar cluster size distribution but uncertainty of the mean size of the clusters.

The photon energies in the measurements were chosen so that overlap of photoelectron peaks with the Auger features would be avoided. The photon energies used for the ionisation of a given electronic level, along with the estimated spectral width of the radiation are tabulated in the lower half of Table 1. The photoelectron spectra were calibrated using the known binding energy of 29.239 eV of the Ar 3*s* atomic line [25]. Experiments on RbCl covered Rb 3*d* binding energy region between 110 eV and 122 eV, Cl 2*p* (200 – 208 eV) as well as Ar 3*s* (27 – 31 eV) for calibration and control purposes. For CsCl, Cs 4*d* binding energy region between 78 eV and 88 eV was investigated along with the same regions of Cl 2*p* and Ar 3*s* as for the RbCl.

Table 1 Operation parameters of the adiabatic expansion source and the I411 beamline: (Upper half) Stagnation pressure P_{stag}, nozzle temperature T_{nozzle}, and predicted mean argon cluster size $\langle N_{\mathrm{Ar}} \rangle$. (Lower half) Photon energy $\hbar\omega$ and estimated spectral width ΔE_{bl}

Sample	P_{stag} [mbar]	T_{nozzle} [K]	$\langle N_{\mathrm{Ar}} \rangle$
RbCl	1500 ± 50	105 ± 5	12000 ± 3000
CsCl	1400 ± 50	85 ± 5	26000 ± 8000
	Region	$\hbar\omega$ [eV]	ΔE_{bl} [meV]
RbCl	Rb 3*d*	196	120
	Cl 2*p*	230	153
CsCl	Cs 4*d*	133	132
	Cl 2*p*	248	338

2.2 Experimental results

2.2.1 Rubidium chloride. Figure 1 presents core-level photoelectron spectra recorded for the RbCl cluster beam. Experimental data points are given by dots. The spectra were recorded at different oven temperatures, which increases from top to bottom. The estimated cluster sizes are indicated for each case. The cluster size estimation method and error limits for the predicted cluster sizes are discussed further down.

Due to the cluster fabrication process used, certain fraction of uncondenced monomers effusing from the oven are always present at the ionisation region. This allows us to make a direct comparison of the cluster response to the parent monomer spectral features. In Fig. 1, the most intense two peaks, denoted as "Mon", belong to the alkali halide monomers. This assignment has been based on a photoelectron spectrum recorded when the Ar clusters were diverted away from the skimmer thus preventing the alkali halide clus-

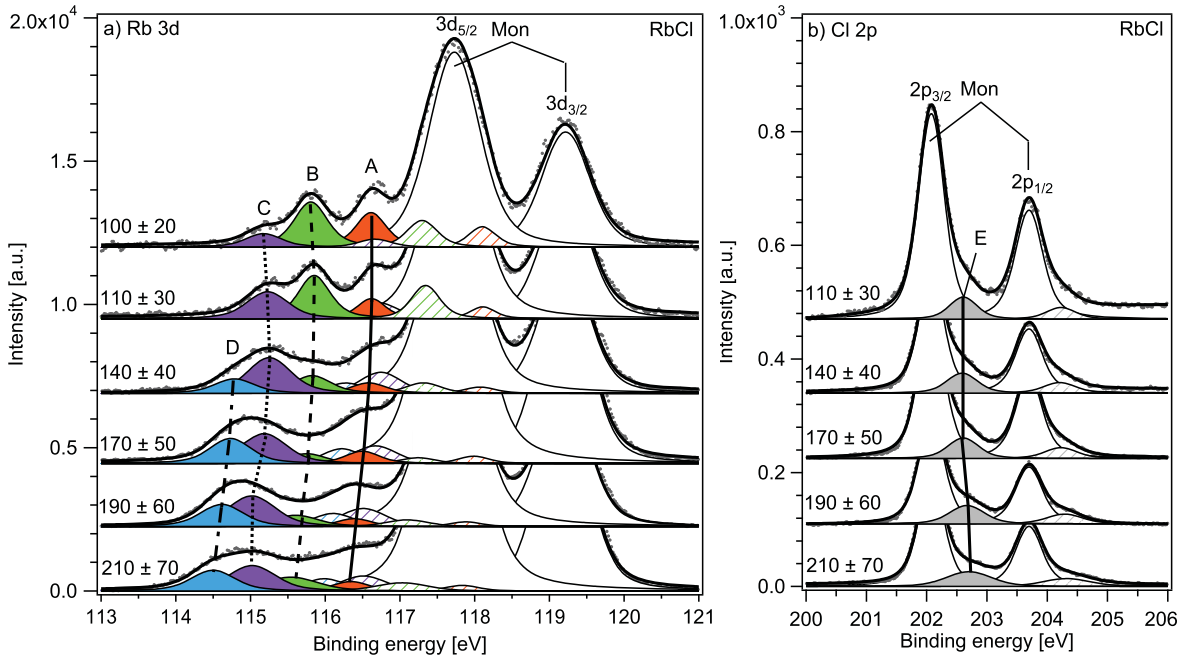

Fig. 1 Photoelectron spectra recorded in a) Rb $3d$ and b) Cl $2p$ regions for RbCl clusters. Estimated mean cluster size is denoted for each spectrum. Rb $3d_{5/2,3/2}$ and Cl $2p_{3/2,1/2}$ monomer related peaks are denoted as "Mon". In Rb $3d$, the cluster response has been fitted with three or four peak doublets where $j = 5/2$ components have been denoted by capital letters A–D and given solid shading while $j = 3/2$ components have striped pattern fill. In Cl $2p$, cluster response has been fitted with only one doublet E. All the spectra have been normalised with respect to the total cluster peak areas. Dots denote the experimental data points while the solid thick line is the sum of the individual peak fits. Vertical lines going through the cluster peaks from A to E are given to guide the eye.

ter formation. The binding energies of the monomer peaks are given in Table 2 as determined by a least-squares spectrum fitting program with symmetric Voigt profiles (Igor Pro by Wavemetrics with SPANCF[26,27] package). All the other peaks denoted by capital letters A–E are due to the alkali halide clusters.

Table 2 Experimentally determined electron binding energies for the alkali chloride monomers. For RbCl M denotes Rb and the main quantum number n = 3, and for CsCl M denotes Cs and n = 4

	RbCl [eV]	CsCl [eV]
M $nd_{5/2}$	117.7(2)	82.7(2)
$nd_{3/2}$	119.2(2)	85.0(2)
Cl $2p_{3/2}$	202.1(1)	202.4(5)
$2p_{1/2}$	203.7(1)	204.0(5)

As can be seen from Fig. 1, the response of the whole cluster beam can be complicated by multiple overlapping peaks. There are several reasons for such complexity. Firstly, the Rb $3d$ level is split by the spin-orbit interaction into $j = 5/2$ and $j = 3/2$ components, and Cl $2p$ into $j = 3/2$ and $j = 1/2$ components. Secondly, the cluster response in itself is composed of signals from atoms in various chemical environments. Starting from the simplest case, the pure monomer spectra in the Rb $3d$ and Cl $2p$ regions (not shown) have been fitted assuming only two peaks, well separated from each other in energy. From this fit, we have calculated the intensity ratio and the binding energy separation (the spin-orbit splitting) for the two peaks in each case - Rb $3d$ and Cl $2p$. The spin-orbit splitting of Rb $3d$ derived from fitting and presented in Table 2 agrees well with the value for atomic rubidium: 1.5 ± 0.1 eV[28,29]. In addition, the fitted Cl $2p$ spin-orbit splitting in RbCl monomer was found to be close to the value of 1.630 ± 0.008 eV[30] known for Cl_2 molecule.

In order to quantify the overlapping cluster responses, the results from the monomer curve fitting have been used to determine the underlying spectral structure. As Rb and Cl have nearly closed electronic shell structure in the monomer $Rb^{(+)}Cl^{(-)}$ form and since spin-orbit splitting is not sensitive to chemical environment, the spin-orbit splitting and the relative intensities of the high- and low-j components of the Rb $3d$ and Cl $2p$ ionised RbCl monomer were taken as fixed parameters in the cluster response fitting.

In the topmost two spectra in Fig. 1 recorded in Rb 3*d* region, three peaks (labeled as A, B, and C) can be distinguished at the lower binding energy side of the monomer $3d_{5/2}$ peak. These have been assigned as the $j = 5/2$ components of the spin doublet. The $j = 3/2$ peaks have been assumed to be at a corresponding separation at the higher binding energy and thus obscured by the $3d_{5/2}$ monomer peak. In the curve fitting, the spin-orbit splitting, the spin-orbit component relative intensity ratios, and the lifetime broadening contribution were fixed to the corresponding values derived from the pure monomer spectra. The parameters left to be optimised for all spin-orbit components (including the monomer) were the Gaussian widths, absolute energy positions and the absolute intensities of the lines.

This procedure was repeated for each spectrum and a total of four peaks for two spin-orbit components arising from the clusters have been assigned in the spectra. Only the lower binding energy components were labeled with A, B, C, or D (solid colour shading) since the other group of spin-orbit components with $j = 3/2$ is not seen under the monomer $3d_{5/2}$ peak and does not bring any additional information due to the fixed spin-orbit splitting and intensity ratio. Still, the fitted lower j components are included in the spectra and denoted by the striped pattern fill. From here on to simplify the discussion, we refer only to the peaks A–D. In the Cl 2*p* side however, the peak fitting has been performed assuming only one doublet, labeled E in Fig. 1b, since no resolved structure has been detected in the cluster response.

In the topmost spectrum in Rb 3*d* region in Fig. 1a, three cluster peaks A–C are visible. As one increases the temperature, the intensity ratios of the peaks change and finally a fourth peak (D) has to be introduced in order the explain the overall cluster response. The individual peaks also experience gradual binding energy shifts towards lower binding energy. This behaviour can be understood as coming from the changing cluster size and it has been widely documented for many types of clusters, including alkali halide clusters[11,16,18,19,31]. With increasing oven temperature, the pick-up rate by the Ar clusters increases which leads to larger alkali halide clusters (see next section for more discussion).

As briefly mentioned above, the Cl 2*p* photoelectron spectra in Fig. 1b are considerably less structured than the alkali metal side. The whole cluster response can be explained with only one doublet (E) which is observed at the higher binding energy side of the monomer lines. This peak broadens and shifts slightly towards the higher binding energies as the cluster size increases. The reason for the difference in the sign of the chemical shift for alkali metal cations and halide anion has been discussed before (see *e.g.* Ref.[16]). Briefly, it can be seen qualitatively to originate due to interplay between the initial and final state (before and after the photoionisation) energies and the way Coulomb interaction affects these states. Much of the following discussion will be concentrated around the cation site (Rb or Cs) spectra but anion spectra are still provided for completeness.

As already discussed in the introduction, earlier theoretical calculations[15,16] predict different chemical shifts for the surface sites of alkali halide clusters according to their coordination where higher coordination leads to correspondingly larger chemical shift. Furthermore, if the sites can be resolved from each other, the intensity of these responses should roughly depend on the number of sites with a given coordination, assuming the mean free path of the emitted photoelectrons is larger than the cluster diameter. The abundance of the low coordination sites diminish and *vice versa* for the high coordination sites as the cluster size increases. Based on all these considerations and the behaviour of the peaks A–D in the experimental photoelectron spectra, these peaks are assigned to the corner (A), edge (B), face (C) and bulk (D) sites of the alkali halide clusters. In general one could argue that the peaks are assigned to ions with different coordination but as many of the alkali halides are known to posses the NaCl structure even as small clusters[15,32], the naming is presumed to be well justified. The assignment of the peak E in the Cl 2*p* spectra is not as straight forward and will be discussed in detail later.

2.2.2 Caesium chloride. In a similar manner, Fig. 2 shows photoelectron spectra recorded in the Cs 4*d* and Cl 2*p* binding energy regions. Due to the qualitatively similar spectra, the assignments are the same as for the RbCl. The CsCl cluster studies have been carried out over a larger oven temperature range.

As with the Rb 3*d*, the Cs 4*d* ionised orbital is spin-orbit split into two components. The energy separation of the monomer Cs $4d_{5/2}$ and $4d_{3/2}$ components given in Table 2 agrees with a previous study[28] on atomic Cs 4*d*, which reports a spin-orbit splitting of 2.29 ± 0.05 eV. As for RbCl cluster assignments in Fig. 1, in Fig. 2 for CsCl the spin-orbit cluster components with the higher j quantum number are denoted with a solid shading and capital letters A–D while the lower j components - with only a stripe pattern.

The Cs 4*d* and Cl 2*p* responses from CsCl clusters have a similar layout to the Rb 3*d* and Cl 2*p* spectra for RbCl ones, respectively. One notable difference is the larger spin-orbit splitting for the monomer Cs 4*d* peaks as was mentioned above. This allows observation of both high- and low-j components of doublet A. As the Rb 3*d* spectra, the Cs 4*d* spectra (Fig. 2a) contain a number of responses with varying relative intensities and to a lesser extent, energy positions. Unlike in bulk RbCl where each of the Rb^+ cations has 6 Cl^- anions in the nearest coordination shell (the NaCl structure), bulk CsCl is well known to posses structure where each Cs^+ cation is 8-fold coordinated with Cl^- anions (thus the name CsCl structure). Although for CsCl the same naming convention as for

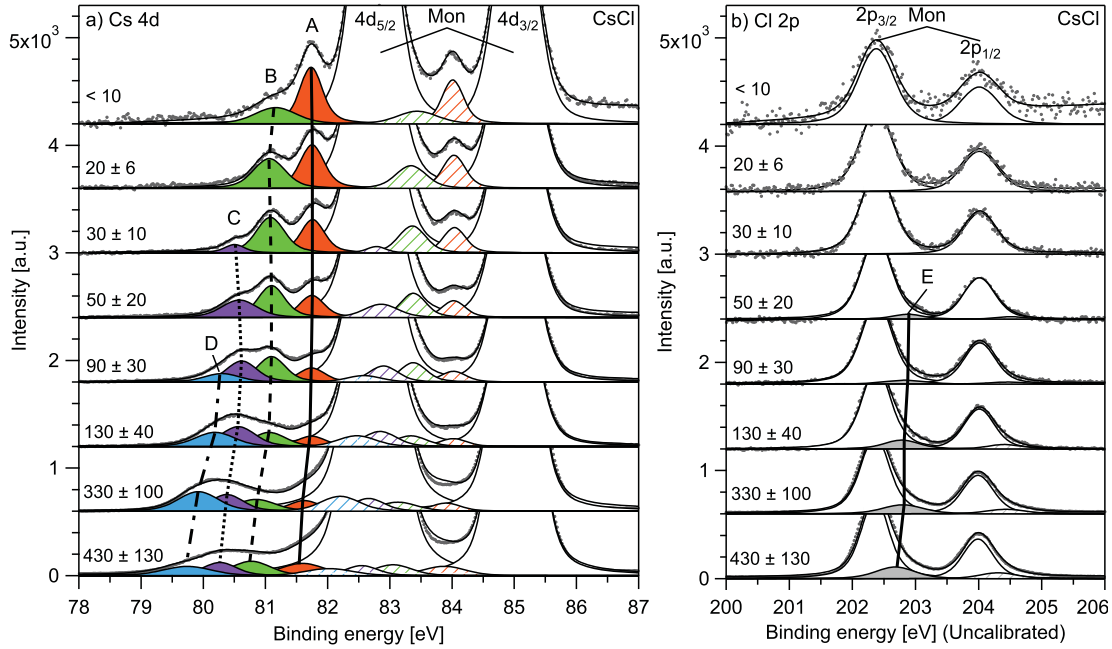

Fig. 2 Photoelectron spectra recorded in a) Cs 4*d* and b) Cl 2*p* regions of CsCl clusters. Estimated mean cluster size is denoted for each spectrum. Cs $4d_{5/2,3/2}$ and Cl $2p_{3/2,1/2}$ monomer related peaks are denoted as "Mon". In Cs 4*d*, the cluster response has been fitted from two to four peak doublets where $j = 5/2$ components have been denoted by capital letters A–D and given solid shading while $j = 3/2$ components have striped pattern fill. In Cl 2*p*, the very weak cluster response has been fitted with only one doublet E. All the spectra have been normalised with respect to the total cluster peak areas. Dots denote the experimental data points while the solid thick line is the sum of the individual peak fits. Vertical lines going through the cluster peaks from A to E are given to guide the eye.

RbCl is used (corner, edge, face, and bulk) for the responses A–D in the CsCl spectra, it does not imply directly that CsCl clusters should posses the same structure as RbCl clusters.

2.3 Alkali halide cluster size estimation

Without using a direct cluster size detection techniques (*e.g.* mass spectrometers) or size selectors, one can rely on theoretical modelling either by considering the size dependent change in the electronic levels of clusters or by predicting the end results of the cluster formation process. For metal clusters, a method based on the relation between the cluster to solid binding energy shift and the cluster size has been used[18,31]. Similar approach has also been suggested for small dielectric particles by Makov *et al.*[33] but in this formulation, the dielectric constant (relative permittivity) of the particle has to be known before one can calculate the particle radius. Monte Carlo simulation was used by Lewerenz *et al.*[34] to model the coagulation of atoms and molecules in large helium clusters formed using similar technique to EXMEC. In the present work we suggest a method which uses similar formalism but does not involve Monte Carlo technique and also omits momentum transfer modelling.

The alkali halide cluster size estimation/modelling proceeds through the following iterative steps:

1. The vapour pressure p_s of the alkali halide is calculated using the temperature T of the oven.
2. Ar cluster diameter d_{Ar} is calculated from the mean (or remaining) Ar cluster size $\langle N_{Ar} \rangle$.
3. Flight distance between successive monomer captures is determined from the mean free path of the Ar cluster.
4. Evaporative loss of Ar atoms upon pick-up of alkali halide monomers is calculated relying on the energy release in the monomer-cluster collision and the alkali halide cluster agglomeration.
5. Steps 2-4 are repeated until the Ar cluster has travelled a distance equal to the pick-up region (oven) length.

No reported solid sublimation pressures were found for the RbCl and CsCl. Therefore the liquid vapour pressures p_l from Ref.[35] were extrapolated to lower than melting point temperatures T_m and then corrected by using a particular form of the

Clausius-Clapeyron equation[36]

$$\ln p_s = \ln p_l - \frac{\Delta H_m}{R}\left(\frac{1}{T} - \frac{1}{T_m}\right), \quad (1)$$

where ΔH_m is the enthalpy of fusion for each of the alkali halides[37], T is the oven temperature and R is the universal gas constant.

The Ar cluster diameter is calculated from the spherical cluster approximation as[38]

$$d_{\mathrm{Ar}} = 2r_{ws}\langle N_{\mathrm{Ar}}\rangle^{1/3} = 2\left(\frac{3M}{4\pi\rho N_A}\right)^{1/3}\langle N_{\mathrm{Ar}}\rangle^{1/3}, \quad (2)$$

where r_{ws} is the Wigner-Seitz radius of Ar, calculated from its molar mass M and liquid density at boiling point[37] of $\rho = 1396\,\mathrm{kg/m^3}$. N_A is the Avogadro constant.

As the mean free path for the individual monomers in the oven is much larger than the mean diameter of the Ar cluster, the latter was assumed to behave as any other molecule in a gas filled volume. Furthermore, as the Ar cluster is larger than the monomer, the cluster diameter is used to define the collision cross-section. Thus, the mean free path for the Ar clusters was calculated by assuming collisions with an ensemble of alkali halide monomers having a Maxwellian speed distribution as

$$\ell = \frac{k_B T}{\sigma p_s}\frac{v_{\mathrm{cluster}}}{\langle v_r\rangle} = \frac{4k_B T}{\pi d_{\mathrm{Ar}}^2 p_s}\frac{v_{\mathrm{cluster}}}{\langle v_r\rangle}, \quad (3)$$

where k_B is the Boltzmann constant, $\sigma = \pi(d_{\mathrm{Ar}}/2)^2$ is the geometric cross section for the Ar cluster representing the collision cross-section, v_{cluster} is the speed of the cluster beam[39] and $\langle v_r\rangle$ is the mean relative speed between the cluster beam and the monomers. These quantities were calculated from

$$v_{\mathrm{cluster}} = \sqrt{\frac{2k_B T_{\mathrm{nozzle}}}{m_{\mathrm{Ar}}}\frac{\gamma}{\gamma - 1}} \quad (4)$$

$$\langle v_r\rangle = \sqrt{v_{\mathrm{cluster}}^2 + \langle v_{\mathrm{mon}}\rangle^2} = \sqrt{v_{\mathrm{cluster}}^2 + \frac{8k_B T}{\pi m_{\mathrm{mon}}}}, \quad (5)$$

where $\gamma = 5/3$ is the specific heat ratio for a monatomic gas (argon), m_{Ar} is the atomic mass of argon, m_{mon} is the atomic mass of the alkali halide monomer and $\langle v_{\mathrm{mon}}\rangle$ is the mean speed of the monomers. In a standard formulation of the mean free path for an ensemble of identical molecules, the ratio $v_{\mathrm{cluster}}/\langle v_r\rangle$ is replaced by a constant value of $2^{-1/2}$. In our calculations with the parameters given, the ratio turned out to be close to this value because the cluster beam speed for Ar is of the same order than the monomer speed.

When the crucible vapour pressure is low, the evaporative loss of Ar is negligible and mean free path of Ar clusters remains constant. As the vapour pressure increases, so does the pick-up rate which increases the Ar evaporation rate. Weak indications of the Ar cluster shrinking were seen during the experiments as increasing surface to bulk signal ratio in the Ar cluster 3*s* photoelectron response, which in previous studies[10,14,40,41] have been resolved also for other rare gas clusters. However, because the energy resolution was not optimised for the Ar 3*s* but for the deeper core-levels in the alkali halides, the surface to bulk response separation remained modest and thus, the uncertainties are significant. The overall Ar 3*s* cluster signal decreased linearly to a point of complete disappearance as the oven temperature was increased, ultimately making the bulk to surface separation in Ar 3*s* impossible for the highest temperatures.

The mean collision energy $\langle E_{\mathrm{col}}\rangle$ is calculated as a sum of the collisional kinetic energy between the monomer and the Ar cluster averaged over all angles and the internal energy of the monomer[34]

$$\langle E_{\mathrm{col}}\rangle = \frac{5}{2}k_B T + \frac{m_{\mathrm{mon}}}{2}v_{\mathrm{cluster}}^2. \quad (6)$$

Binding energy of 6.82 eV per monomer addition for CsCl[42] was used to describe the heat released by agglomeration. The RbCl monomer binding energy of 7.2 eV was interpolated from the values of NaCl (7.92 eV[42]) and CsCl. Bulk enthalpy of vaporisation of Ar[37] (6.447 kJ/mol) was taken to approximate the energy needed to release Ar atoms from the cluster. With these assumptions, pick-up of each alkali halide monomer evaporated roughly 90-110 Ar atoms.

The calculated size range extended from 100 to 210 atoms/cluster for RbCl and from <10 to 430 atoms/cluster for CsCl as indicated in Figs. 1 and 2. The error estimates of the alkali halide cluster sizes are completely based on the Ar cluster size error limits given in Table 1. Validity of this model is investigated in the discussion section.

3 Computations

3.1 Computational methods

In order to get more information on the origin of the photoelectron peaks assigned to different sites of the cluster response, binding energy shift (chemical shift) calculations with respect to free monomer cases were performed. The binding energy shifts between the monomer and clusters were calculated using a simple ground-state potential model (GPM) and more involved relaxation-potential model (RPM) introduced by Davis and Shirley[43–45]. In GPM the shift is taken to be the difference between the (reference) potential of the monomer and the potential in the cluster calculated at corner, edge, face or bulk sites. The binding energy shift ΔE_b thus takes the form $\Delta E_b = -(V_a^{\mathrm{Ref}} - V_a^{\mathrm{Cluster}})$, where

$$V_a = \sum_i \langle\psi_i|r_{ia}^{-1}|\psi_i\rangle - \sum_{j\neq a} Z_j/R_{ja}. \quad (7)$$

The summation index i runs over all occupied single electron wavefunctions ψ_i in the calculation. The second term accounts for the potential created by the nuclei Z_j, omitting the nucleus at position a. The model yield the same shift for all orbitals of the same site and it was originally developed to give estimations for K-shell chemical shifts. However, it seems to work fairly well for higher orbitals as well (as long as the orbital is local on the studied site). This assumption is further justified by the recent experimental observation that the chemical shifts in metallic clusters do not vary significantly between different core orbitals[31].

The RPM improves GPM by adding term $-\Delta V_r$ representing the contribution from the relaxation of the wavefunctions at the final singly ionized state. The term is given by equation $V_r = 1/2(V_a^+ - V_a)$, where V_a^+ is the potential at site a with electronic wavefunctions ψ_i^+ calculated in $Z_a + 1$ nuclear potential. Note that in GPM all binding energy shifts are obtained from a single calculation, whereas in RPM the wavefunctions have to be optimised for each studied site individually. In the original papers of the model[43–45], CNDO wavefunctions were used with some further simplifications. Due to the development of computational resources, the present calculations were done by computing directly the potentials V_a from (7) with Hartree-Fock wavefunctions and Gaussian basis sets.

The electronic wavefunctions were obtained by using the Orca quantum chemistry program (version 2.9.1)[46]. The calculations were performed in single configuration Hartree-Fock scheme using the Ahlrichs-VDZ basis sets[47] with effective-core potentials for Rb and Cs[48]. The rather small basis set was chosen due to dramatic increase of computational time and instabilities in convergence for larger cluster sizes. The calculations were however checked with Ahlrichs-TZVP basis for small cluster sizes and the binding energy shifts did not change considerably. The clusters were assumed to have a NaCl crystal structure, which has been found to be the lowest-energy geometry for small alkali halide clusters (see, *e.g.* Refs.[32,49,50] and references therein). The bond length of 3.285 Å for RbCl clusters was taken to be the experimental value derived from bulk RbCl[51]. Since CsCl does not have NaCl structure in the bulk form, a bond length value of 3.571 Å based on geometry optimisation of an $(CsCl)_4$ $(2 \times 2 \times 2)$ cluster was used for CsCl clusters. The reference RbCl and CsCl monomer bond lengths were taken from the experimental values of the monomer[52].

3.2 Computational results

Results of the GPM (upper row) and RPM (lower row) calculations are collected into Fig. 3. As all the clusters were assumed to have the NaCl lattice structure, the sites (and their number of nearest neighbours) that appear in the geometry are located at the corner (3), edge (4), face (5), or bulk (6) of the cluster. In Fig. 3 the calculated cluster to monomer binding energy shifts ΔE_b are shown as a function of the cluster configurations. Because clusters with the same number of cations and anions were considered, $i \times j \times k =$ even for all the configurations. In this notation scheme, the indices i, j, and k give the number of atoms along each of the three mutually perpendicular edge directions. The values of the shifts are averages of the slightly differing chemical shifts of the atoms belonging to the same coordination but different positions in the cluster.

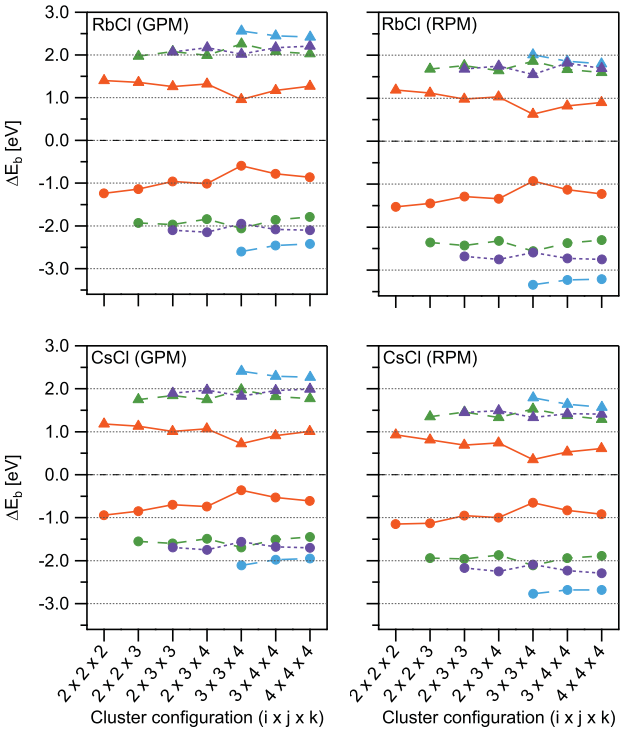

Fig. 3 Calculated binding energy shifts ΔE_b for the RbCl and CsCl clusters as a function of cluster configuration. Results have been computed with (RPM) and without (GPM) the final state relaxation. Triangles represent binding energy shifts for the halogen (chlorine) ions and circles for the alkali metal ions (Rb or Cs). Sites are separated by the use of orange (corner), green (edge), purple (face), and blue (bulk) lines.

The calculations predict negative binding energy shifts, *i.e.* towards lower binding energies relative to the monomer, for the alkali metal cations and positive shifts for the halogen anions. For the different sites, the absolute values of the shifts increase from the corner ion site with lowest coordination to the bulk site with the highest coordination. An exception to this order is observed for the $3 \times 3 \times 4$ configuration, where the edge and face site chemical shifts switch order. This is

most likely linked to the appearance of the first bulk site to the configuration which changes the local potential momentarily. Both the Coulomb interaction between ions and the charge induced dipole interaction depend on the coordination of the site in question which qualitatively explains the site order as described more thoroughly by Zhang *et al.* [16].

For both alkali metal and halogen ions, the chemical shift of the corner site stands apart from the rest, which more or less group together. The grouping is more pronounced in the halogen ion sites than in the alkali-metal ion sites. In addition, different sites in RbCl tend to be more separated in energy from each other than in the CsCl. The binding energy shifts are slightly larger in magnitude for the RbCl than for the CsCl but the results for the two compounds are quite similar.

In the RPM the alkali metal cation binding energy shifts are larger and the halogen anion shifts smaller in comparison to the GPM. Moreover in RPM, the edge, face and bulk sites are more densely grouped for the halogen ions, whereas the alkali-metal sites become more separated in energy.

In both models the overall trend of the binding energy shifts as a function of cluster size is quite flat. The calculated shifts especially for the smallest cluster configurations should be seen more as orientating rather than accurate predictions since geometry optimisation was not performed. In some previous studies on small alkali halide clusters [15,49], the latter were shown to adopt geometries that did not resemble bulk NaCl structures. As the cluster size increases NaCl structures become more probable and the shift values can be assumed to converge towards the values calculated for the largest $4\times4\times4$ clusters.

4 Discussion

The experimental results show that the core-level photoelectron response from alkali halide clusters evolves in shape and size significantly as the cluster size changes in a relatively narrow range below one-two hundred atoms/cluster. The computational results indicate that the structures seen in the alkali metal (Rb and Cs) spectra originate from the different surface sites (corner, edge, and face) and from the bulk of the cluster.

4.1 Binding energy shifts

The binding energy shifts between the monomer and the different cluster peaks obtained by fitting the experimental spectra have been plotted in Fig. 4 for the RbCl and CsCl as a function of the estimated mean cluster size. The error bars for the shifts were derived from the Gaussian FWHM's of the fitted peaks after subtracting the beamline and analyser broadening contributions from it. The corresponding standard deviation was then used to describe the uncertainty of each peak's position. Cluster size error bars have been left out for the sake of clarity but can be found from Figs. 1 and 2.

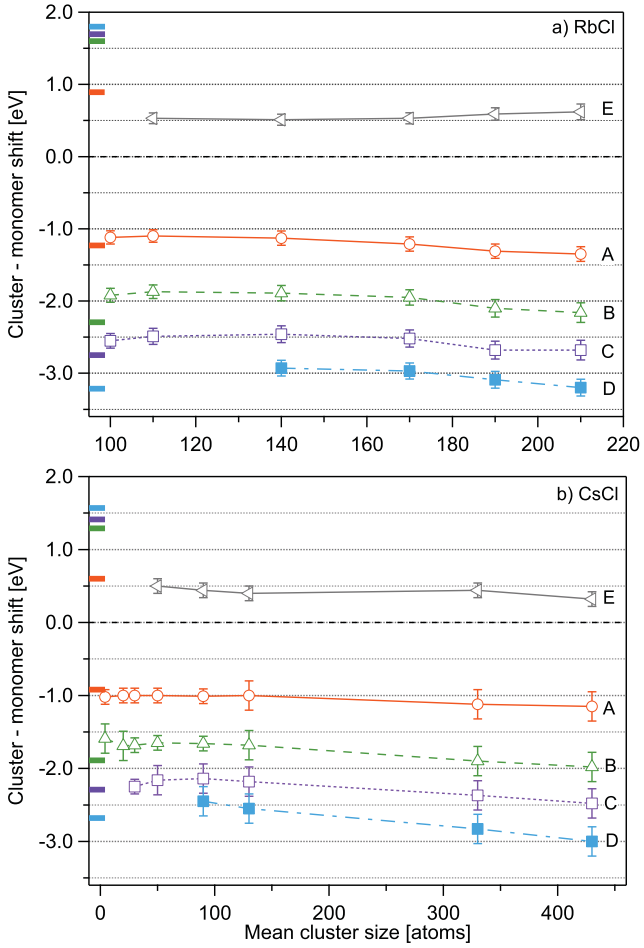

Fig. 4 Experimental cluster to monomer binding energy shifts for a) RbCl and b) CsCl as derived by curve fitting from the spectra presented in Figures 1 and 2. Markers for shift values (and the corresponding peaks in the spectra) are as follows: Circles (A), upward pointing triangles (B), hollow squares (C), solid squares (D), and left pointing triangles (E). The calculated binding energies of the $4\times4\times4$ cluster from the RPM are shown as small horizontal ticks beside the binding energy axis.

The chemical shifts of Rb 3d levels for RbCl clusters in Fig. 4a range from -1.1 eV for the peak A to -3.2 eV for the peak D. Calculated shifts for the $4\times4\times4$ cluster are presented as small ticks beside the vertical energy scale. A small overall shift towards lower binding energies is observed in the values as the mean cluster size increases. The magnitude of the binding energy shifts for the peaks A, B, C, and D correspond quite well to the calculated shifts of the RPM for the corner, edge, face, and bulk sites presented in Fig. 3, respectively. Similar analysis of the CsCl in Fig. 4b shows that the Cs 4*d* shifts

(peaks A–D) are slightly smaller than the corresponding shifts in Rb 3*d* ranging from −1.0 eV (peak A) to −3.0 eV (peak D). This difference in the overall shift magnitude between the two alkali metals is also predicted by the calculations.

The chemical shift of the halogen anion in RbCl and CsCl is considerably smaller in magnitude than any of the alkali metal cation shifts. The only cluster related peak (E) in Cl 2*p* retains a positive shift of about 0.5 eV which is in line with previous work on NaCl[16] and KCl[19] reporting binding energy shifts of about +1 eV and +0.7 eV, respectively. The decreased anion binding energy shift across the chloride series can be qualitatively seen as resulting from the increasing interionic distance when moving from NaCl to CsCl which decreases the Coulomb interaction. Even though the calculations predict that the corner site should be resolvable from the other sites, no other peaks are seen in the spectra. It is possible that the corner peak is overlapping with the monomer signal, but the reason can be as well that the chemical shift is overestimated by the calculation and the corner response is bunched together with the other peaks. We may speculate that it is due to the limitation of the single determinant HF approximation as well as insufficiently included final state orbital relaxation.

The total chemical shift for an ion in a particular site in the alkali halide cluster is influenced by the Coulomb interaction, the polarisation interaction and the repulsive overlap of nearby atomic orbitals (see *e.g.* Refs.[16,19] and references therein). The binding energy shift caused by these interactions scales as a function of coordination. For NaCl lattice the coordination ranges from 3 (corner site) to 6 (bulk site). If the peaks observed in the photoelectron spectra of clusters originate from different sites (corner, edge, face, or the bulk) as the calculations suggest, ratios of the shift values could reflect the coordination on each site.

As a case in point, binding energy shift ratios of the alkali metal region cluster peaks from RbCl and CsCl are shown in Fig. 5. For all the sites, each binding energy shift value has been divided by the edge site shift. These have been scaled so that the edge site ratio always corresponds to 4. As can be observed from the figure, the face and bulk site ratios coincide with their expected coordination (5 and 6) when the edge site coordination is fixed. Since the three sites are so evenly spaced in binding energy, fixing the ratio for any of the three sites produces qualitatively identical results. The corner site however deviates from the predicted coordination of 3 throughout the measured spectra and acquires a value of approximately 2.5. The smaller than expected binding energy shift for the corner site could be a result of site dependent changes such as decreasing polarisability of ions, especially anions, with increasing coordination as proposed by Zhang *et al.*[19].

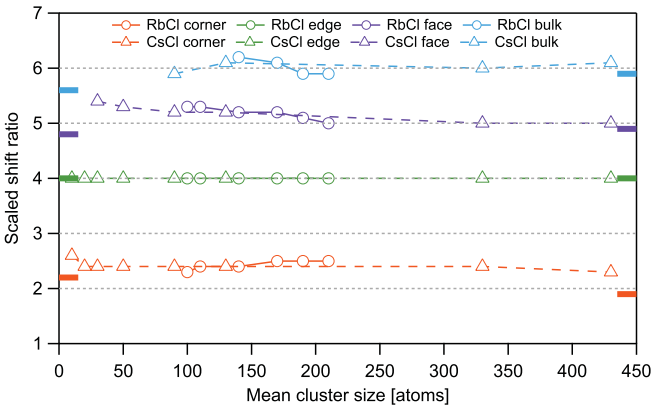

Fig. 5 Scaled binding energy ratio as a function of mean cluster size. The ratio has been calculated by dividing the individual site binding energy shifts with the edge site shift value and then by multiplying it with 4, corresponding to the edge site coordination in NaCl structure. Circles represent the RbCl and triangles the CsCl data. Shift ratios based on the computational results for the $4 \times 4 \times 4$ are shown on the left (RbCl) and right (CsCl) of the figure as thick horizontal ticks.

4.2 Site fractions

As follows from our results presented in Figs. 1 and 2, the relative intensities of peaks A–D change as a function of cluster size. Since each peak corresponds to one coordination site in the cluster, the intensity ratios, or site fractions from here on, are proportional to the number of atoms occupying the sites of the cluster (assuming that the size of the cluster is smaller than the photoelectron escape depth). The site fractions change as a function of cluster size and geometry. As the cluster beam contains multiple sizes, the photoelectron spectrum is a superposition of sets of site fractions. By comparing the experimental site fractions to the statistically derived ones, one can gain insight about the (average) cluster geometry. For size selected clusters one could even detect individual isomers as proposed by Aguado *et al.*[15]

Figure 6 shows calculated site fractions for two different crystal structures. The upper panel presents NaCl structure and the lower panel bcc rhombic dodecahedron structure (referred as CsCl structure[32]). In order to account for the size distribution in the experiment, each NaCl site fraction was formed by taking an ensemble of clusters with a Gaussian size distribution and a standard deviation given by the present mean cluster size. For the CsCl structure, site fractions were calculated for full rhombic dodecahedral atomic shell closings where the number of shells goes from 1 to 5.

Label $i \times j \times k$ denotes the number of atoms along each edge. Only configurations with at least one even edge index were considered as the clusters were assumed to be composed

of diatomic molecules. Also configurations with large edge index differences (such as $6 \times 2 \times 2$) were discarded as being improbable in the experiment, since cubes and closely related cuboids tend to be more stable[42].

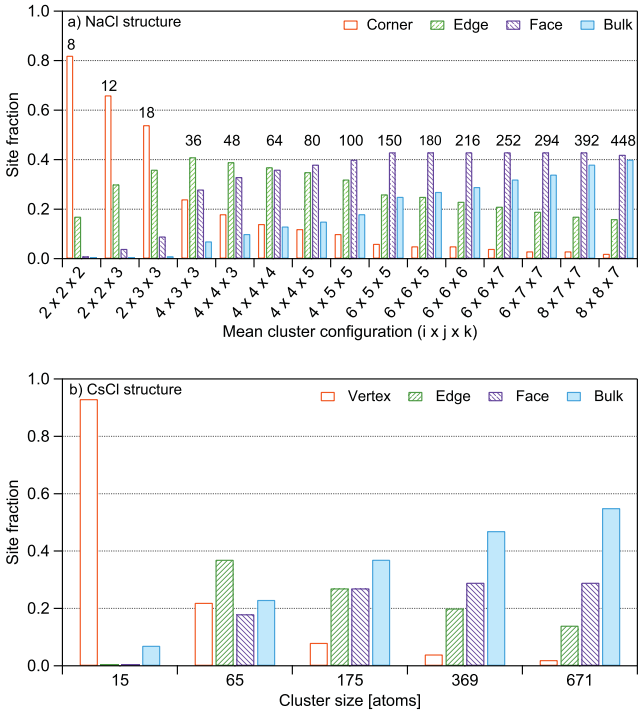

Fig. 6 Calculated site fractions for a) NaCl structure and b) bcc rhombic dodecahedron (CsCl) structure. In the upper panel, mean cluster configurations are given under the horizontal axis and the mean cluster sizes are indicated above the columns. Cluster sizes in the lower panel are exact (see text for details).

Figure 7 shows the experimentally derived site fractions as a function of the estimated mean cluster size. Error bars estimate the oscillation in the fitted peak areas during the curve fitting procedure. A vertical dashed line in the site fraction plots labeled *saturation point* (SP) denotes a point were the Ar cluster signal vanishes from the photoelectron spectra completely. This point is always achieved when high enough pick-up oven temperature (vapour pressure) is reached. As can be seen from the CsCl site fractions in Fig. 7b and photoelectron spectra in Fig. 2, even though the Ar cluster signal has disappeared in the last spectrum beyond the saturation point, the alkali halide cluster signal is still present, although with a slightly reduced intensity. If the oven temperature is decreased, the Ar cluster signal recovers. This is an indication of the fact that after a certain point, the saturation point, nearly all or all of the Ar atoms have evaporated from the cluster and the evaporative cooling mechanism is removed. This is also predicted by the alkali halide cluster size estimation procedure.

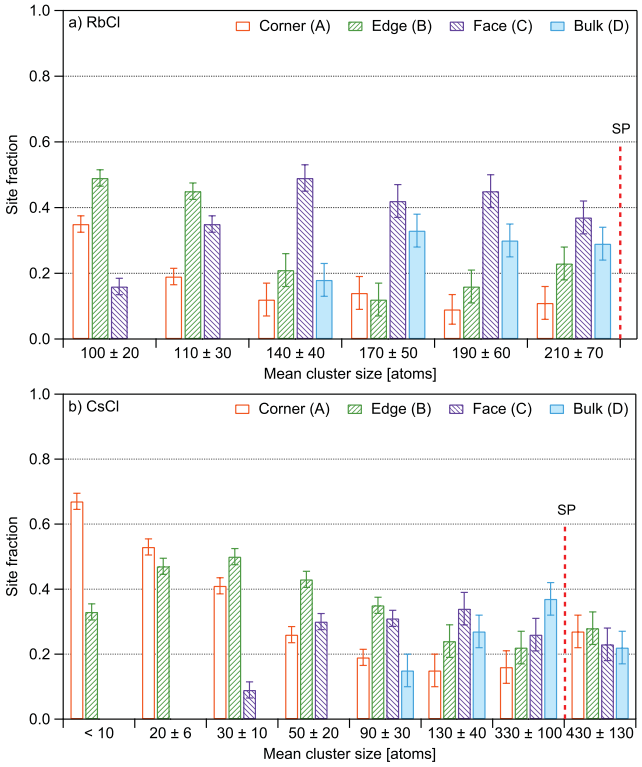

Fig. 7 Experimentally determined relative peak areas, denoted as site fractions, for a) RbCl and b) CsCl. The capital letters refer to the peaks observed in the photoelectron spectra. The point at which the Ar cluster signal disappears from the photoelectron spectra almost completely is marked with a vertical dashed line and an abbreviation SP which stands for saturation point.

The experimental RbCl site fractions quantitatively follow from the simple consideration that the low-coordination site fractions decrease with the size. One can suggest a method for size estimation based on the comparison of the experimental and calculated site fractions. For RbCl, this method seems to overestimate the size of the smallest clusters but the agreement improves somewhat for the largest sizes. Overall the behaviour of the experimental site fractions can be explained by the NaCl structure.

In the case of CsCl the cluster size range is larger than for RbCl and starts at around 10 atoms/cluster. This allows observing both the initial increase and the slow decrease of the edge site fraction. For smaller clusters (up to about 90 atoms/cluster) the experimental site fraction distributions reflect the statistical distributions of NaCl structure fairly well, which allows us to conclude that CsCl clusters have a NaCl structure in this size range. On the other hand, in the case of larger clusters (from size about 130 atoms/cluster onwards) the experimental signal from the bulk sites increases notice-

ably. This behaviour could be understood assuming the appearance of a significant concentration of clusters with CsCl structure in the interaction region as a previous study has placed the structural phase transition point from NaCl to CsCl structure at around 370 atoms/cluster[32]. Figure 6b shows that for rhombic dodecahedral structure the bulk site fraction dominates from around 150 atoms/cluster onwards which is in close agreement with the experimental observations.

The largest cluster size of 430 atoms presents some peculiar behaviour. The corner and edge fractions have increased whereas the face and bulk fractions have decreased. This behaviour could be explained by the assumption of formation of surface terraces which are built onto the complete cluster faces. These additional low coordination sites would decrease the face site fraction in the favour of corner and edge sites. Also, previous mass spectroscopic studies[42] have found evidence of such structures in the corresponding size range. Signal suppression due to inelastic scattering of photoelectrons could also play a part in the decreasing bulk site fraction, particularly at the largest cluster sizes in the experiment.

5 Conclusions

The present results demonstrate the possibility to gather site specific information from multicomponent clusters using photoelectron spectroscopy. The observed responses in the core-level photoelectron spectra of RbCl and CsCl clusters were linked to different atomic coordination sites. By monitoring the surface site signals as a function of cluster size, information about the cluster geometry was deduced. The chemical shift data provided information about the local, site-specific interaction mechanisms and indicated a non-linear scaling of the binding energy shifts observed for the different sites which could be associated to the changes in the electron structure such as ion site dependent polarisabilities[19].

The RbCl clusters were seen to display site fraction patterns typical for a bulk NaCl structure. Similar association to this structure was also made for the smaller CsCl clusters, whereas the largest clusters contained evidence that a significant fraction of the clusters in the beam possessed the bulk CsCl structure.

Applications of the presented technique could include chemical reaction analyses on the surface of free clusters in a manner similar to single crystal surface catalysis studies. These kind of studies would provide interesting insights to site-specific catalytic processes.

Acknowledgements

The experiments were performed at MAX-lab (Sweden) at the I411 beamline during two beamtimes (proposal numbers 20120165 and 20130121). EXACTUS doctoral program (University of Oulu) and Jenny and Antti Wihuri foundation are gratefully acknowledged by L. Hautala for their support. The authors would like to acknowledge the financial support from the Academy of Finland. The research leading to these results has received funding from the European Community's Seventh Framework Programme (FP7/2007-2013) CALIPSO under grant agreement no 312284. The authors would also like to thank the MAX-lab staff for their assistance during the experiments.

References

1 C. C. Pradzynski, R. M. Forck, T. Zeuch, P. Slavicek and U. Buck, *Science*, 2012, **337**, 1529–1532.
2 O. Lopez-Acevedo, K. A. Kacprzak, J. Akola and H. Häkkinen, *Nat. Chem.*, 2010, **2**, 329–334.
3 K. Yamamoto, T. Imaoka, W.-J. Chun, O. Enoki, H. Katoh, M. Takenaga and A. Sonoi, *Nat. Chem.*, 2009, **1**, 397 – 402.
4 K. C. L. Black, Y. Wang, H. P. Luehmann, X. Cai, W. Xing, B. Pang, Y. Zhao, C. S. Cutler, L. V. Wang, Y. Liu and Y. Xia, *ACS Nano*, 2014, **0**, in press.
5 W. Xiong, D. D. Hickstein, K. J. Schnitzenbaumer, J. L. Ellis, B. B. Palm, K. E. Keister, C. Ding, L. Miaja-Avila, G. Dukovic, J. L. Jimenez, M. M. Murnane and H. C. Kapteyn, *Nano Lett.*, 2013, **13**, 2924–2930.
6 M. Kulmala, I. Riipinen, M. Sipilä, H. E. Manninen, T. Petäjä, H. Junninen, M. Dal Maso, G. Mordas, A. Mirme, M. Vana, A. Hirsikko, L. Laakso, R. M. Harrison, I. Hanson, C. Leung, K. E. J. Lehtinen and V.-M. Kerminen, *Science*, 2007, **318**, 89–92.
7 F. Postberg, S. Kempf, J. Schmidt, N. Brilliantov, A. Beinsen, B. Abel, U. Buck and R. Srama, *Nature*, 2009, **459**, 1098–1101.
8 A. W. Castleman, Jr. and S. N. Khanna, *J. Phys. Chem. C*, 2009, **113**, 2664–2675.
9 W. Eberhardt, *Surf. Sci.*, 2002, **500**, 242–270.
10 T. Hatsui, H. Setoyama, N. Kosugi, B. Wassermann, I. L. Bradeanu and E. Rühl, *J. Chem. Phys.*, 2005, **123**, 154304.
11 O. Björneholm, F. Federmann, F. Fössing and T. Möller, *Phys. Rev. Lett.*, 1995, **74**, 3017–3020.
12 P. S. Bagus, F. Illas, G. Pacchioni and F. Parmigiani, *J. Electron Spectrosc. Relat. Phenom.*, 1999, **100**, 215–236.
13 H. Bergersen, M. Abu-samha, J. Harnes, O. Björneholm, S. Svensson, L. J. Sæthre and K. J. Børve, *Phys. Chem. Chem. Phys.*, 2006, **8**, 1891–1898.
14 M. Tchaplyguine, R. R. Marinho, M. Gisselbrecht, J. Schulz, N. Mårtensson, S. L. Sorensen, A. Naves de Brito, R. Feifel, G. Öhrwall, M. Lundwall, S. Svensson and O. Björneholm, *J. Chem. Phys.*, 2004, **120**, 345–356.
15 A. Aguado, A. Ayuela, J. M. Lòpez and J. A. Alonso, *Phys. Rev. B*, 1998, **58**, 9972–9979.
16 C. Zhang, T. Andersson, S. Svensson, O. Björneholm, M. Huttula, M.-H. Mikkelä, M. Tchaplyguine and G. Öhrwall, *J. Chem. Phys.*, 2011, **134**, 124507.
17 M. Patanen, C. Nicolas, X.-J. Liu, O. Travnikova and C. Miron, *Phys. Chem. Chem. Phys.*, 2013, **15**, 10112.
18 M. Huttula, M.-H. Mikkelä, M. Tchaplyguine and O. Björneholm, *J. Electron Spectrosc. Relat. Phenom.*, 2010, **181**, 145–149.
19 C. Zhang, T. Andersson, S. Svensson, O. Björneholm, M. Huttula, M.-H. Mikkelä, D. Anin, M. Tchaplyguine and G. Öhrwall, *J. Phys. Chem. A*, 2012, **116**, 12104–12111.

20 L. Partanen, M.-H. Mikkelä, M. Huttula, M. Tchaplyguine, C. Zhang, T. Andersson and O. Björneholm, *J. Chem. Phys.*, 2013, **138**, 044301.

21 M. Bässler, A. Ausmees, M. Jurvansuu, R. Feifel, J.-O. Forsell, P. de Tarso Fonseca, A. Kivimäki, S. Sundin, S. L. Sorensen, R. Nyholm, O. Björneholm, S. Aksela and S. Svensson, *Nucl. Instr. Meth. Phys. Res.*, 2001, **469**, 382–393.

22 M. Bässler, J.-O. Forsell, O. Björneholm, R. Feifel, M. Jurvansuu, S. Aksela, S. Sundin, S. L. Sorenssen, R. Nyholm, A. Ausmees and S. Svensson, *J. Electron Spectrosc. Relat. Phenom.*, 1999, **101-103**, 953–957.

23 F. Dorchies, F. Blasco, T. Caillaud, J. Stevefelt, C. Stenz, A. S. Boldarev and V. A. Gasilov, *Phys. Rev. A*, 2003, **68**, 023201.

24 U. Buck and R. Krohne, *J. Chem. Phys.*, 1996, **105**, 5408.

25 A. Kramida, Y. Ralchenko, J. Reader and NIST ASD Team, NIST Atomic Spectra Database (ver. 5.1), [Online]. Available: `http://physics.nist.gov/asd` [2014, May 20]. National Institute of Standards and Technology, Gaithersburg, MD., 2013.

26 E. Kukk, G. Snell, J. D. Bozek, W.-T. Cheng and N. Berrah, *Phys. Rev. A*, 2001, **63**, 062702.

27 E. Kukk, K. Ueda, U. Hergenhahn, X.-J. Liu, G. Prümper, H. Yoshida, Y. Tamenori, C. Makochekanwa, T. Tanaka, M. Kitajima and H. Tanaka, *Phys. Rev. Lett.*, 2005, **95**, 133001.

28 S. Fritzsche, K. Jänkälä, M. Huttula, S. Urpelainen and H. Aksela, *Phys. Rev. A*, 2008, **78**, 032514.

29 K. Jänkälä, J. Schulz, M. Huttula, A. Calò, S. Urpelainen, S. Heinäsmäki, S. Fritzsche, S. Svensson, S. Aksela and H. Aksela, *Phys. Rev. A*, 2006, **74**, 062704.

30 O. Travnikova, R. F. Fink, A. Kivimäki, D. Céolin, Z. Bao and M. N. Piancastelli, *Chem. Phys. Lett.*, 2006, **426**, 452–458.

31 M.-H. Mikkelä, M. Tchaplyguine, S. Urpelainen, K. Jänkälä, O. Björneholm and M. Huttula, *J. Appl. Phys.*, 2012, **112**, 084326.

32 A. Aguado, *Phys. Rev. B*, 2000, **62**, 13687.

33 G. Makov, A. Nitzan and L. E. Brus, *J. Chem. Phys.*, 1988, **88**, 5076.

34 M. Lewerenz, B. Schilling and J. P. Toennies, *J. Chem. Phys.*, 1995, **102**, 8191.

35 C. L. Yaws, *Handbook of vapor pressure, volume 4: Inorganic compounds and elements*, Gulf publishing company, 1995.

36 B. Moller, J. Rarey and D. Ramjugernath, *J. Mol. Liq.*, 2008, **143**, 52–63.

37 *CRC Handbook of chemistry and physics*, ed. W. M. Haynes, Taylor & Francis Group, 95th edn, 2014.

38 R. L. Johnston, *Atomic and molecular clusters*, Taylor & Francis Group, 1st edn, 2002.

39 H. Pauly, *Atom, Molecule and Cluster Beams I: Basic Theory, Production and Detection of Thermal Energy Beams*, Springer, 1st edn, 2000.

40 U. Hergenhahn, S. Barth, V. Ulrich, M. Mucke, S. Joshi, T. Lischke, A. Lindblad, T. Rander, G. Öhrwall and O. Björneholm, *Phys. Rev. B*, 2009, **79**, 155448.

41 M. Lundwall, H. Bergersen, A. Lindblad, G. Öhrwall, M. Tchaplyguine, S. Svensson and O. Björneholm, *Phys. Rev. A*, 2006, **74**, 043206.

42 Y. J. Twu, C. W. S. Conover, Y. A. Yang and L. A. Bloomfield, *Phys. Rev. B*, 1990, **42**, 5306.

43 D. W. Davis and D. A. Shirley, *Chem. Phys. Lett.*, 1972, **15**, 185–190.

44 D. W. Davis, M. S. Banna and D. A. Shirley, *J. Chem. Phys.*, 1974, **60**, 237.

45 D. W. Davis and D. A. Shirley, *J. Electron Spectrosc. Relat. Phenom.*, 1974, **3**, 137–163.

46 F. Neese, *Wiley Interdiscip. Rev.: Comput. Mol. Sci.*, 2012, **2**, 73–78.

47 A. Schäfer, H. Horn and R. Ahlrichs, *J. Phys. Chem.*, 1992, **97**, 2571.

48 T. Leininger, A. Nicklass, W. K. Küchle, H. Stoll, M. Dolg and A. Bergner, *Chem. Phys. Lett.*, 1996, **255**, 274.

49 A. Aguado, A. Ayuela, J. M. Lòpez and J. A. Alonso, *Phys. Rev. B*, 1997, **56**, 15353.

50 P. C. R. Rodrigues and F. M. S. Silva Fernandes, *Eur. Phys. J. D*, 2007, **44**, 109–116.

51 R. W. G. Wyckoff, *Crystal structures*, Wiley, 1964, vol. 1.

52 L. R. Maxwell, S. B. Hendricks and V. M. Mosley, *Phys. Rev.*, 1937, **52**, 968.